TIGIT expression dictates the immunosuppressive reprogramming of myeloid cells in glioblastoma.

Mohammad Asad[1], Julio Inocencio[1], Stefan Mitrasinovic[1], Minori Aoki[1], Celina Crisman[1], Patrick Lasala[1], Emad Eskandar[1], Chandan Guha[2], XingXing Zang[3], Ian F. Parney[4], and Benjamin T. Himes[1*]

[1]Department of Neurological Surgery, Albert Einstein College of Medicine/Montefiore Medical Center; Bronx, NY, 10461, USA (Mohammad Asad, J.I., S. M., Minori Aoki, C.C., P.L., E.E.)

[2]Department of Radiation Oncology, Albert Einstein College of Medicine/Montefiore Medical Center; Bronx, NY, 10461, USA (C.G.)

[3]Department of Microbiology & Immunology, Albert Einstein College of Medicine/Montefiore Medical Center; Bronx, NY, 10461, USA (X.Z.)

[4]Department of Neurological Surgery, Mayo Clinic; Rochester, MN, 55905, USA (I.F.P.)

Running title: TIGIT drives immunosuppression in glioblastoma

*Corresponding author. Email: Dr. Benjamin T. Himes

Albert Einstein College of Medicine, Department of Neurological Surgery; Kennedy-530, 1410 Pelham Parkway S. Bronx, NY, 10461, USA

Email ID: bhimes@montefiore.org

Phone number: +1 (718) 430-2538

Manuscript word count (includes abstract, text, references, and figure legends):

TIGIT expression dictates the immunosuppressive reprogramming of myeloid cells in glioblastoma.

Mohammad Asad, Julio Inocencio, Stefan Mitrasinovic, Minori Aoki, Celina Crisman, Patrick Lasala, Emad Eskandar, Chandan Guha, XingXing Zang, Ian F. Parney, and Benjamin T. Himes

Abstract

Glioblastoma (GBM) is a deadly brain cancer with near-universal recurrence despite maximal treatment for which new innovations are sorely needed. Immunotherapy has yet to make significant gains in GBM treatment despite revolutionizing other cancer therapies, due in part to GBM-mediated immune suppression. This immune derangement proceeds through several mechanisms, but increasing evidence points to critical roles for tumor-derived extracellular vesicles (EVs) and immunosuppressive myeloid cells as key factors in this process. In the present study, we demonstrate broad expression of TIGIT across myeloid cell populations in the GBM microenvironment, a finding recapitulated by conditioning healthy monocytes with GBM-derived EVs. Further, knockdown of TIGIT expression reduced the immunosuppressive polarization of monocytes, resulting in improvement in T cell function. This finding proceeded in an NLRP3-dependent manner, with substantial co-localization of TIGIT and NLRP3 expression prior to knockdown. These findings point to a novel role for TIGIT expression in diverse myeloid cells in the GBM microenvironment as a marker of immunosuppressive activity and further indicate a hierarchy of immunomodulatory protein activity in these myeloid cells, with TIGIT knockdown unmasking the pro-inflammatory activity of NLRP3. This study bolsters understanding of the

immunosuppressive complexities of myeloid cells in the GBM microenvironment, while lending further support to prevention or attenuation of immunosuppressive myeloid cell activity as a means of restoring immune function in GBM.

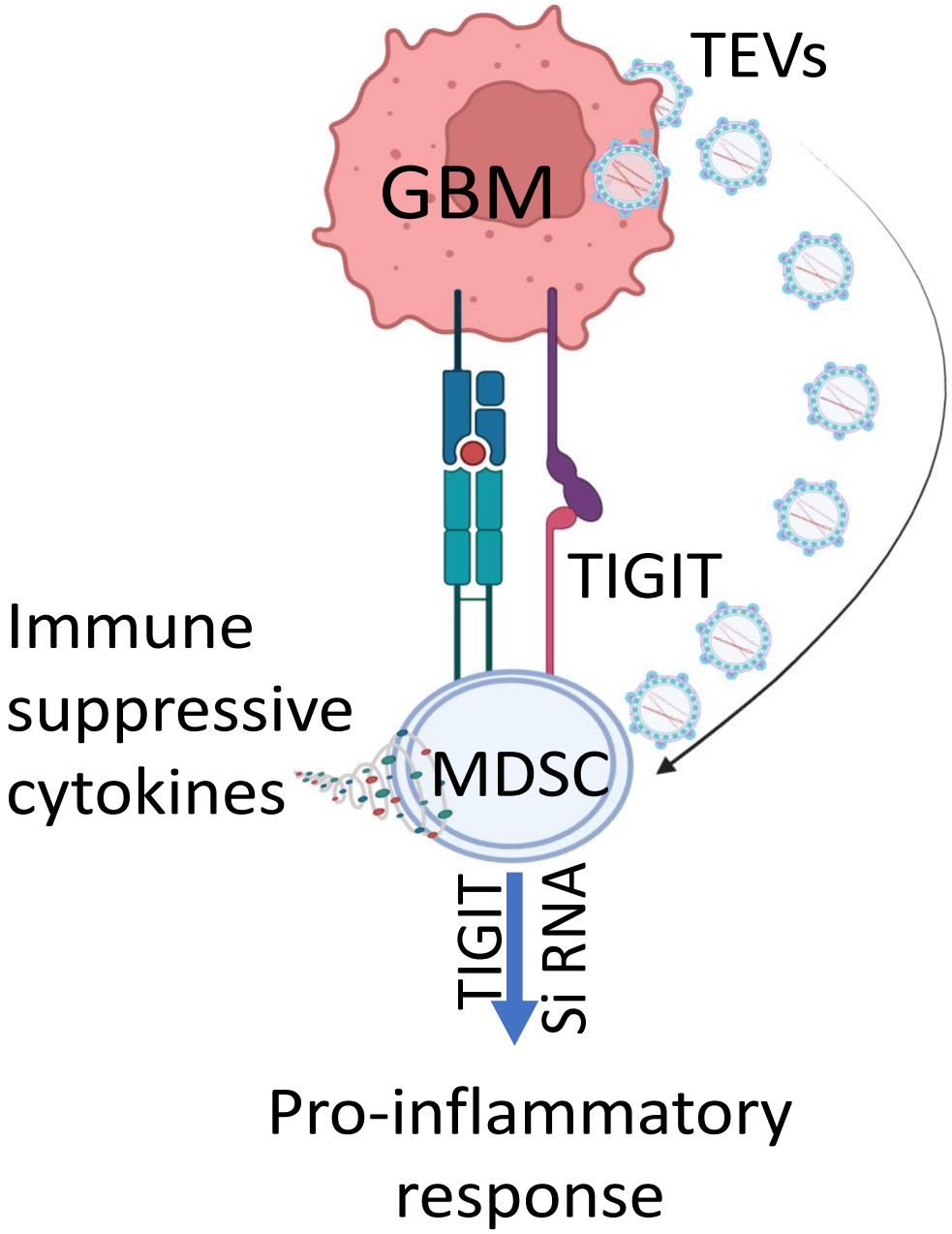

Graphical abstract (Created in BioRender. Asad, M. (2025) https://BioRender.com/euiljoq

Keywords

glioblastoma, TIGIT, extracellular vesicles, immunotherapy, myeloid cell, NLRP3

Key Points

1. TIGIT is broadly expressed in myeloid cells within the GBM microenvironment and can be induced by GBM-derived extracellular vesicles.
2. Knockdown of TIGIT reduces immunosuppressive polarization of monocytes and enhances T cell activity via NLRP3 signaling.
3. This study advocates immunomodulatory hierarchy in GBM, positioning TIGIT as a potential therapeutic target to reverse immune suppression.

Importance of the Study

Glioblastoma (GBM) remains a formidable clinical challenge, with poor prognosis and limited response to current immunotherapies. This study uncovers a novel immunosuppressive axis involving TIGIT expression in myeloid cells, which are key players in the GBM tumor microenvironment. By demonstrating GBM-derived extracellular vesicles induce TIGIT in healthy monocytes and TIGIT knockdown diminishes immunosuppressive polarization via an NLRP3-dependent pathway, the study highlights TIGIT as both a marker and modulator of immune dysfunction in GBM. These findings introduce a functional hierarchy of immunoregulatory proteins in tumor-associated myeloid cells, positioning TIGIT as a potential checkpoint target. Restoring immune activity by disrupting this axis could enhance the efficacy of immunotherapy in GBM. Thus, this research not only advances our understanding of tumor-induced immune suppression but also opens a promising therapeutic avenue to reinvigorate

71 anti-tumor immunity in a cancer type historically resistant to immunotherapeutic
72 approaches.

73 **Introduction**

74 Glioblastoma (GBM) is the most common and deadly intrinsic brain tumor in adults.
75 Current standard of care consists of maximal safe surgical resection followed by
76 radiation and temozolomide chemotherapy, in a protocol essentially unchanged for two
77 decades (*1*). Some recent innovations, such as tumor treating fields, have shown
78 modest promise but have not led to increased median overall survival beyond 15
79 months in population-based studies (*2*). Immunotherapy, including immune checkpoint
80 blockade, has been transformative in cancer care in recent years, but has failed to
81 improve outcomes in GBM (*3-6*). The profound immunosuppression found in GBM
82 patients plays a critical role in these failures, but its underlying mechanisms remain
83 poorly understood (*6, 7*).

84 Increasing evidence points to a crucial role for myeloid cells, which can comprise the
85 bulk of the tumor immune infiltrate, as mediators of immune suppression, preventing the
86 antitumor effects of T cells (*7, 8*). These myeloid cells are heterogenous with and
87 include a number of distinct populations, including myeloid-derived suppressor cells
88 (MDSCs) and non-classical monocytes (NCM) (*8-12*). These diverse populations are
89 united by the common trait of facilitating immune suppression, whether by release of
90 immunosuppressive cytokines or expression of surface ligands that facilitate exhaustion
91 of effector cells, including T cells (*7, 13*).

92 The mechanisms by which GBM induces immunosuppression are multiple and an active
93 field of study, but an increasing body of work points to a central role of tumor-derived
94 extracellular vesicles (EVs) (*7, 10, 14, 15*). These complex, multimodal signaling
95 molecules, are shed by all cells and play a critical role in cancer signaling, particularly in
96 immune evasion (*16*). In GBM, work by our group and others has pointed to a
97 potentially pivotal role of EVs in tumor-mediated immune suppression, including the
98 induction of immunosuppressive myeloid cells (*10, 14, 17*). Thus, the means by which
99 GBM induces the immunosuppressive polarization of myeloid cells represents a
100 potentially potent therapeutic axis for mitigation of GBM-mediated immune suppression.

101 In the present study, we examine the immune phenotype of myeloid cells in the GBM
102 tumor microenvironment at the time of surgical resection using ultrasonic aspirate
103 processed directly from the operating room to identify immunomodulatory markers
104 expressed across diverse myeloid cell populations that may represent therapeutically
105 significant targets across diverse cell populations. Interestingly, we found high rates of
106 TIGIT (T cell immunoreceptor with immunoglobulin and ITIM domain). TIGIT is increasingly
107 recognized as playing a critical role in limiting adaptive and innate immunity and is
108 canonically understood as a marker for T cell exhaustion. Recent data demonstrates
109 TIGIT expression across an array of myeloid cells in the *in- situ* GBM microenvironment
110 (*18-20*). These findings were recapitulated using our *in vitro* system of
111 immunosuppressive monocyte induction, whereupon healthy monocytes are subjected
112 to GBM-EVs collected from patient-derived cell lines. Upon knockdown of TIGIT
113 expression in monocytes, we found cells underwent a more pro-inflammatory immune
114 polarization in response to EV conditioning. TIGIT knockdown unmasked high levels of

115 co-expressed NLRP3 and increased levels of IL-13 expression. This resulted in a
116 rescue of T cell proliferation upon subsequent co-culture, indicating a level of functional
117 restoration of immune function. These results illustrate the potentially crucial role of an
118 immunomodulatory hierarchy in myeloid cells in the tumor microenvironment, the
119 understanding of which may prove critical for reversal of tumor-mediated immune
120 suppression.

121 **Results**

122 **Immunophenotyping of myeloid cells in the GBM microenvironment reveals**
123 **broad TIGIT expression**

124 GBM is an intrinsic infiltrative tumor, with the radiographic tumor bulk comprised of
125 heterogenous tumor cells, immune infiltrate, and normal brain cells. Surgical resection
126 of GBM entails removing as much of the lesion as safely possible with a range of
127 surgical techniques, frequently including liberal use of an ultrasonic aspirator, which
128 breaks up the bulk tumor and allows for resection without excess trauma due to heat or
129 retraction on the surrounding brain. The ultrasonic aspirate from this approach thus
130 consists of all of the constituent cells of the bulk tumor and is thus a valuable source of
131 material for study of the *in situ* tumor microenvironment, as well as tumor cells for
132 primary cell culture and establishment of patient-derived cell lines. Ultrasonic aspirate
133 from 13 GBM patients was collected and the immune cell infiltrate profiled via high
134 dimensional flow cytometry (Cytek Aurora, full panel and gating strategy available in
135 **Table S1 and Fig. 1**). Analysis of a number of key immunomodulatory proteins were
136 assessed across several known immunosuppressive monocyte populations, including
137 monocytic myeloid-derived suppressor cells (mMDSCs,

Fig. 1

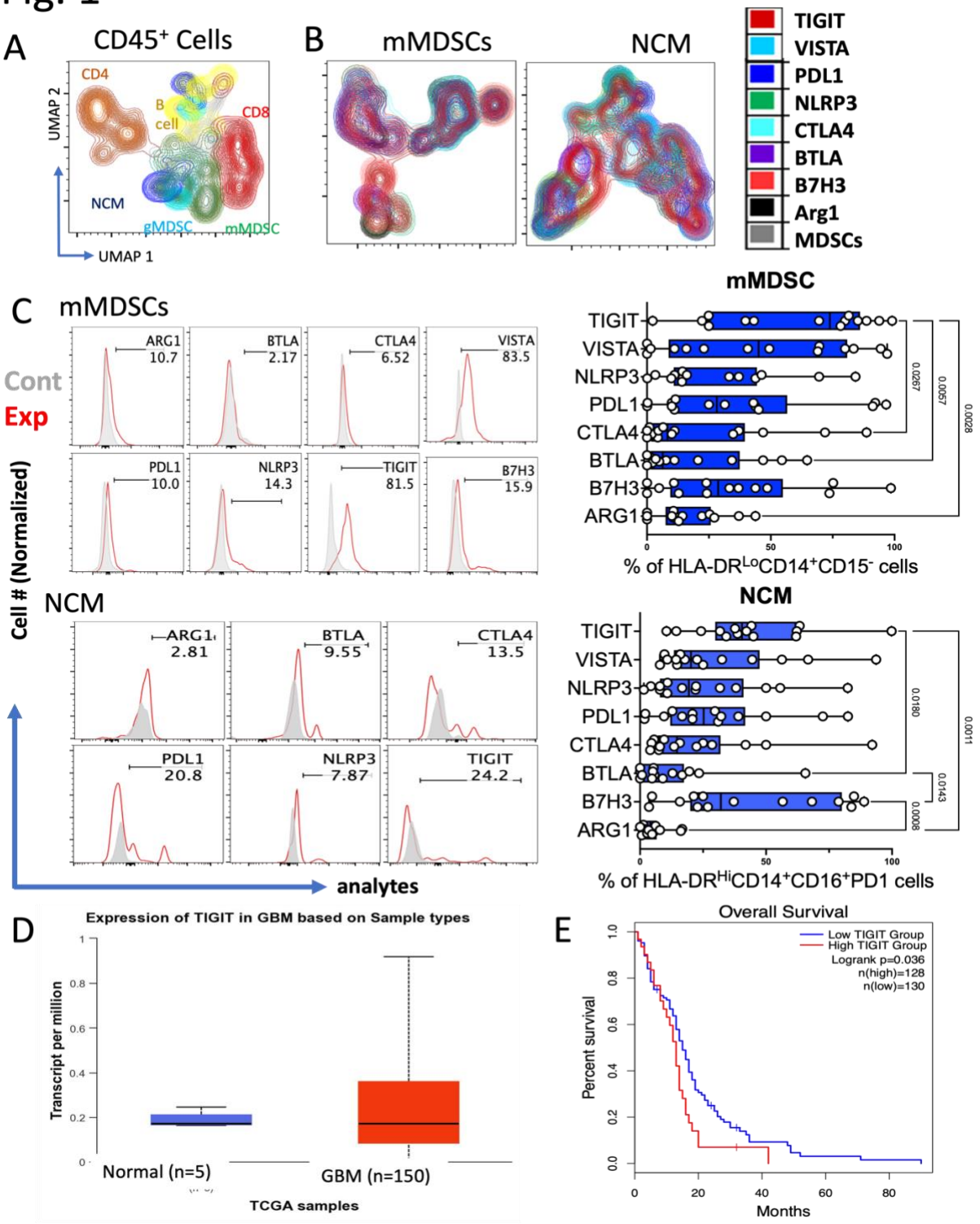

138

139 **Figure 1: Expression of immune modulatory molecules by suppressive monocytes of GBM**

140 **patients.** For surveying the tumor-immune microenvironment in samples of ultrasonic aspirates collected

during surgery, samples were processed for flow cytometric studies and the single cell suspensions, stained with various flow antibodies were run on Cytek aurora spectral flow cytometer. (**A**) UMAP analysis of CD45+ cells from GBM patients show various infiltrating immune cells. (**B**) Showing the cellular expression of immune modulatory molecules (TIGIT, PDL1, NLRP3, BTLA, CTLA4, ARG1) by infiltrating immune suppressive monocyte subsets, monocytic Myeloid Derived Suppressor Cells, mMDSCs ($CD45^{+}CD11b^{+}CD15^{-}HLA\text{-}DR^{Lo}CD14$ cells) and nonclassical monocytes (NCM, $CD45^{+}CD11b^{+}CD15^{-}HLA\text{-}DR^{+}CD14^{-}PD1^{+}CD16$ cells). (**C**) Histograms and a corresponding summary bar graph depicting the immune modulatory molecules expressing cell population in mMDSCs and NCM. (**D**) Box plot obtained from TCGA database illustrates the expression of TIGIT in normal and primary tumor samples obtained from GBM patients. (**E**) Kaplan-Meier curve of TCGA and GTEx datasets of human GBM, demonstrating the effect of TIGIT expression on patient survival in GBM. Data are presented as mean ± s.e.m. and were analyzed by one-way analysis of variance (ANOVA) with Tukey's multiple comparisons.

$CD11b^{+}CD15^{-}CD14^{+}HLA\text{-}DR^{lo/-}$) and non-classical monocytes (NCM, $CD11b^{+}CD15^{-}CD16^{+}HLA\text{-}DR^{+}PD\text{-}1^{+}$), that have been previously described as major populations of immunosuppressive myeloid cells in the GBM microenvironment (**Fig. 1A**) (*10, 14, 21*). Among the infiltrating immune cells, T cells constituted the largest population, followed by immunosuppressive monocytes and B cells. Subsequent analysis of immunomodulatory proteins in mMDSC and NCM populations revealed enriched expression of a few key immune modulatory proteins, such as VISTA, PD-L1 and B7-H3 (**Fig. 1B, C**). Interestingly, we found that TIGIT, typically thought of as a T cell exhaustion marker, was significantly elevated in elevated in immunosuppressive myeloid cell populations relative to other immunomodulatory markers. Despite the significant presence of PD-L1 (29.75±5.83%) and B7-H3 (50.34±9.093%) expressing cells in NCM, $TIGIT^{+}$ cells predominated among the myeloid cell populations within the various suppressive monocytic subsets (64.27±7.99% and 39.8±4.366% in mMDSCs

166 and NCM respectively). Analysis of The Cancer Genome Atlas (TCGA) data
167 demonstrated enrichment of TIGIT expression across several GBM samples. Further,
168 TCGA and GTEx datasets of human GBM was analyzed using Gene Expression
169 Profiling Interactive Analysis. The TIGIT high group (top 20%, N= 128) indicated in red
170 showed a significant worse overall survival than the TIGIT low group (the rest 80%, N=
171 130) in blue, p = 0.036 (**Fig. 1 D, E**). Thus, it appears that elevated TIGIT mRNA
172 expression is associated with poor survival in human GBM patients.

173 **GBM-EVs recapitulate myeloid cell immunosuppressive polarization *in vitro***

174 We next sought to validate these findings outside of the highly heterogenous context of
175 the tumor microenvironment. Work by our group and others has pointed to a major role
176 for GBM-derived extracellular vesicles (EVs) in the formation of immunosuppressive
177 monocytes (*10*). We previously demonstrated that EVs collected from patient-derived
178 GBM cell cultures can induce the formation of immunosuppressive monocytes, including
179 mMDSCs and NCMs, when used to condition monocytes collected from healthy human
180 blood donors. Using these techniques, we collected GBM-EVs from three patient-
181 derived GBM cell lines (dBT114, dBT116, and dBT120). In order to collect EVs, GBM
182 cells were cultured in serum-free conditions for 72hr and subjected to staged
183 centrifugation as described above. Presence and sizing of EVs was confirmed by use of
184 the NanoSight Nanotracker system (ZetaView, Particle Matrix, Germany) as well as the
185 presence of the EV markers CD9 and CD63 via western blot (**Fig. 2A-C**). EV
186 quantification was performed by BCA assay to quantify total protein. To induce the
187 formation of immunosuppressive monocytes, 20ug of EVs was added to monocytes

Fig. 2

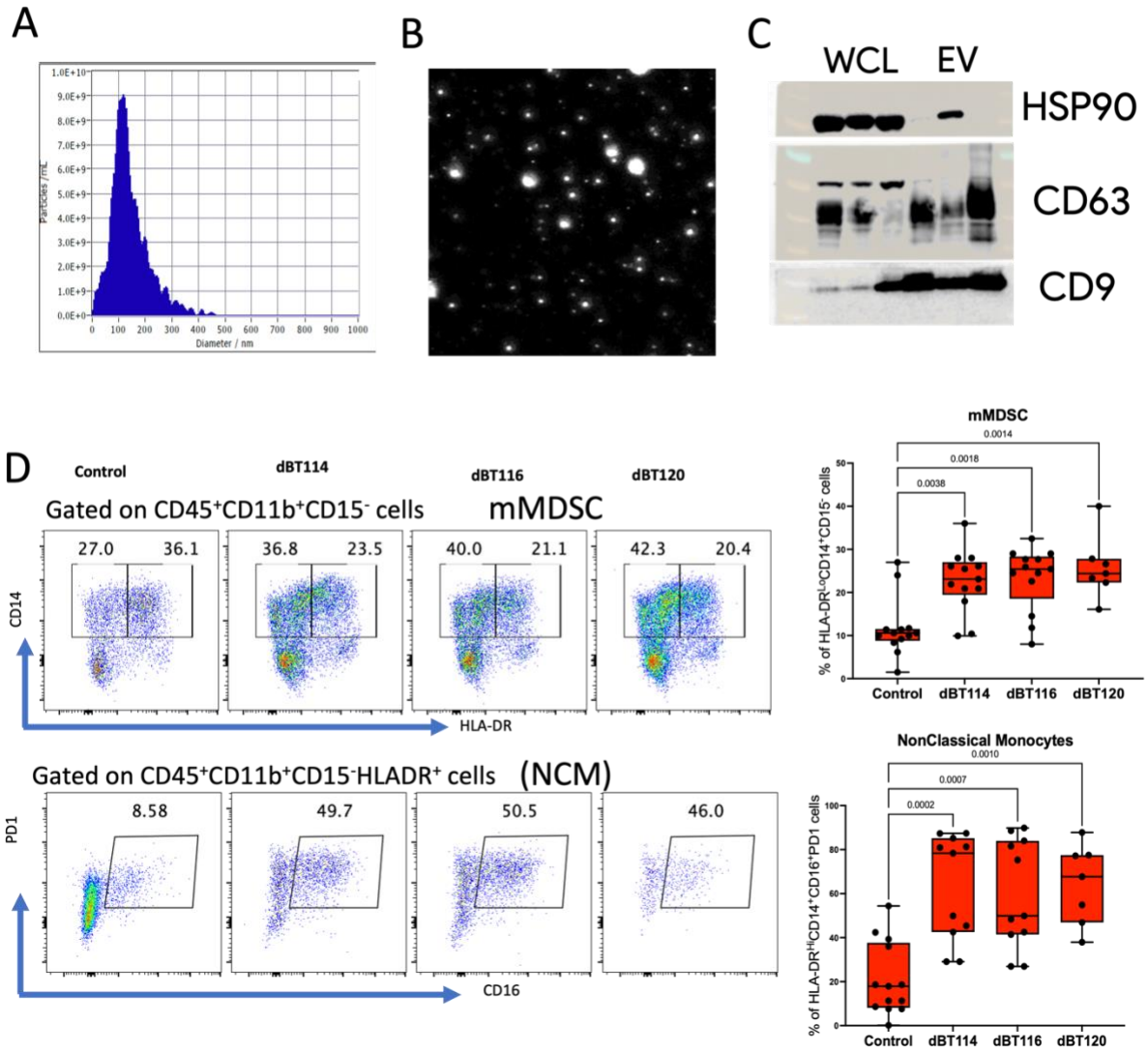

188

189 **Figure 2: Isolation and characterization of tumor-derived extracellular vesicles (TEVs) and**

190 **induction of immune suppressive monocytes.** Extra cellular vesicles from human GBM primary cells

191 lines were obtained by ultracentrifugation and characterized by Nano-sight and western blots. (**A**) Size

192 distribution analysis of tumor-derived extracellular vesicles (TEVs) isolated from conditioned medium post

193 ultracentrifugation. (**B**) Representative image depicting the shape and relative size of the heterogeneous

194 TEVs, obtained from Nano-sight. (**C**) Western blot analysis of TEVs and whole cell lysate (WCL) for the

195 presence of CD63, and CD9 as TEVs markers. (**D**) CD11b^{+} cells, isolated from healthy PBMCs and

196 induced with control or different TEVs isolated from primary GBM cell lines (dBT114, dBT116 and
197 dBT120) under hypoxic condition in serum free medium. After 72 hours, cells were collected and
198 processed for flow cytometry and stained with various fluorochorm tagged antibodies. Flow cytometric
199 analysis of monocytic Myeloid Derived Suppressor Cells (mMDSCs, $CD45^{+}CD11b^{+}CD15^{-}HLA\text{-}DR^{Lo}CD14$
200 cells and nonclassical monocytes (NCM, $CD45^{+}CD11b^{+}CD15^{-}HLA\text{-}DR^{+}CD14^{-}PD1^{+}CD16$ cells) isolated
201 from healthy PBMCs and induced with control or different TEVs isolated from primary GBM cell lines.
202 Data are presented as mean ± s.e.m. and were analyzed by one-way analysis of variance (ANOVA) with
203 Tukey's multiple comparisons.

204 isolated from anonymous healthy blood donors (obtained from the New York Blood
205 Bank). Monocytes were conditioned with EVs for 72h in hypoxic (1% O2) conditions
206 prior to collection for flow cytometry analysis (panel included in **S2**). Consistent with our
207 previously published results, EVs derived from dBT114, dBT116, and dBT120 all
208 significantly induced the formation of both mMDSCs and NCM in this model system
209 (**Fig. 2D**), which produce anti-inflammatory cytokines including IL-4 (**Fig. S2**).

210 Using this model, we next employed a high-dimensional flow cytometry approach as
211 employed for the ultrasonic aspirate samples to define the expression pattern of
212 immunomodulatory proteins in this model. We found substantial similarities in
213 immunomodulatory protein expression following EV-conditioning of monocytes,
214 including consistent increases in TIGIT and NLRP3 expression (**Fig. 3A**, **B**). TIGIT
215 expression was increased in both mMDSCs (73.53±6.27%, 68.33±8.66% and
216 63.99±8.11% respectively for the mentioned cell lines EVs, compared to unstimulated
217 control, 4.68±2.83%) and NCM (85.17±3.91%, 79.26±9.17% and 60.68±10.52%
218 respectively, compared to control, 11.3±3.3%) following treatment with EVs derived from

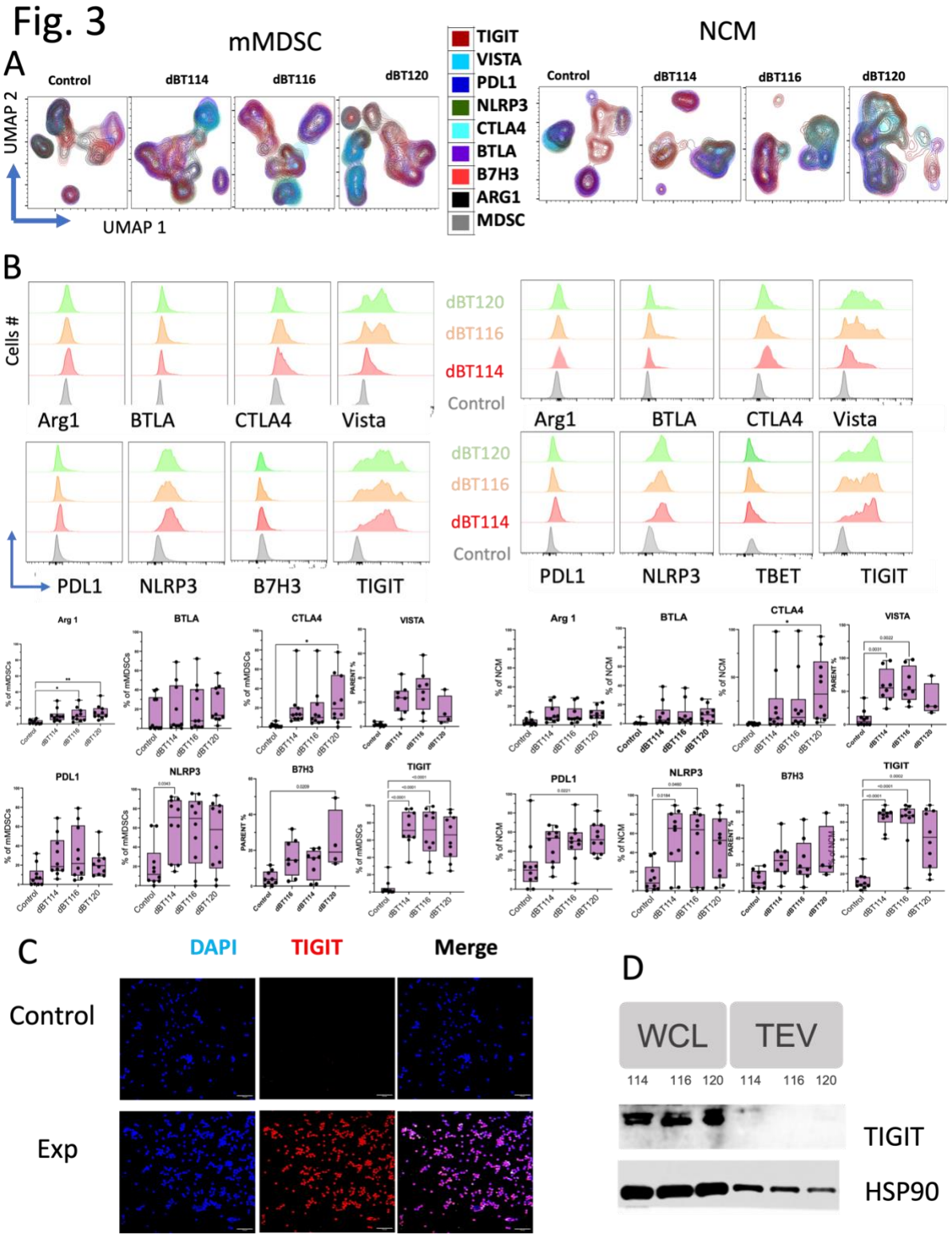

Figure 3: Expression of immune modulatory molecules on TEVs induced peripheral monocytic Myeloid Derived Suppressor Cells (mMDSC) & non-classical monocytes (NCM). CD11b^{+} cells,

222 isolated from healthy peripheral blood and under hypoxic condition in a serum free medium, co-cultured
223 for 72 hours with TEVs obtained from mentioned GBM cell lines. (**A**) TEVs induced CD11b^{+} monocytes
224 were studied for the expression of various immune modulatory markers, TIGIT, PDL1, NLRP3, BTLA,
225 CTLA4 & ARG1 on suppressive monocyte subsets (mMDSCs and NCMs). (**B**) Histograms depicting the
226 expression levels of immune modulatory molecules on mMDSC and NCM populations cultured with
227 control or different TEVs (dBT114, dBT116 and dBT120). The percentage of cells expressing each
228 molecule within each subset is also shown correspondingly as a chart. (**C**) Immunofluorescence staining
229 of TIGIT in suppressive monocytes treated with control or TEVs. (**D**) Western blot analysis of GBM whole
230 cell lysate (WCL) for the presence of TIGIT. Data are presented as mean ± s.e.m. and were analyzed by
231 one-way analysis of variance (ANOVA) with Tukey's multiple comparisons.

232 all three GBM cell lines. We confirmed that TIGT expression in this model was present
233 in monocytes and not from co-localized EVs via western blot demonstrating TIGIT
234 expression in GBM whole cell lysate (WCL), but not in EVs (**Fig. 3C**). Further,
235 immunofluorescent staining following EV-monocyte co-culture for 72h demonstrated
236 robust TIGIT expression in monocytes conditioned with EVs, but not in untreated
237 controls, demonstrating that hypoxic culture conditions, which have previously been
238 shown to aid in MDSC induction, were insufficient to induce TIGIT expression (**Fig. 3D**).

239 **TIGIT and key immunomodulatory proteins are co-expressed in EV-induced**
240 **immunosuppressive monocyte populations**

241 While there is some recent work describing TIGIT expression in myeloid cells (*20*),
242 typically TIGIT has been viewed as a T cell exhaustion marker, and so it is not
243 necessarily intuitive that high levels of TIGIT expression on immunomodulatory myeloid
244 cells corresponds to downstream immunosuppressive functionality in myeloid cells. We,
245 therefore next interrogated the immunomodulatory proteins and cytokines co-expressed

246 on TIGIT+ immunosuppressive monocytes. Several other immune-checkpoint markers,
247 including PD-L1 and VISTA, demonstrated high levels of co-expression on TIGIT
248 positive mMDSCs and NCM following GBM-EV treatment (**Fig. 4A, B,** representative
249 dot plots for co-localization included in **Fig. S3**). Interestingly, NLRP3, typically
250 understood as a strong marker of pro-inflammatory activity important in the
251 inflammasome pathway, demonstrated the strongest amount of co-expression. It is
252 noteworthy that among all $CD45^+$ cells, $TIGIT^+$ cells showed a significantly higher
253 expression of $NLRP3^+$ cells (86.64±5.52%) compared to other immunomodulatory
254 molecules, including Arg1 (0.45±0.14%), BTLA (2.2±0.94%), CTLA-4 (27.34±11.12%),
255 and PD-L1 (48.09±4.41%) (Fig. S3c). This elevated NLRP3 expression was
256 accompanied by a significant increase in IL-1β-producing cells (55.88±5%), an
257 inflammatory cytokine associated with NLRP3, as well as IL-13-producing cells
258 (98.78±.3%). These levels were notably higher than those of the proinflammatory
259 cytokines IFNγ (7.3±2.65%) and IL-17 (1.63±0.63%), and the immunosuppressive
260 cytokines IL-4 (5.9±1.3%), IL-5 (16.98±5%), and IL-10 (12.49±2.35%) (**Fig. S3**). In
261 interrogating a panel of key cytokines, we found that the TH2 cytokine, IL-13 was co-
262 expressed with TIGIT expression on immunosuppressive monocytes (**Fig. 4C, D)**.
263 Taken together, these findings suggest that an immunosuppressive phenotype prevails
264 in the presence of co-expressed pro-inflammatory markers in EV-induced
265 immunosuppressive monocytes, suggestive of an

Fig. 4

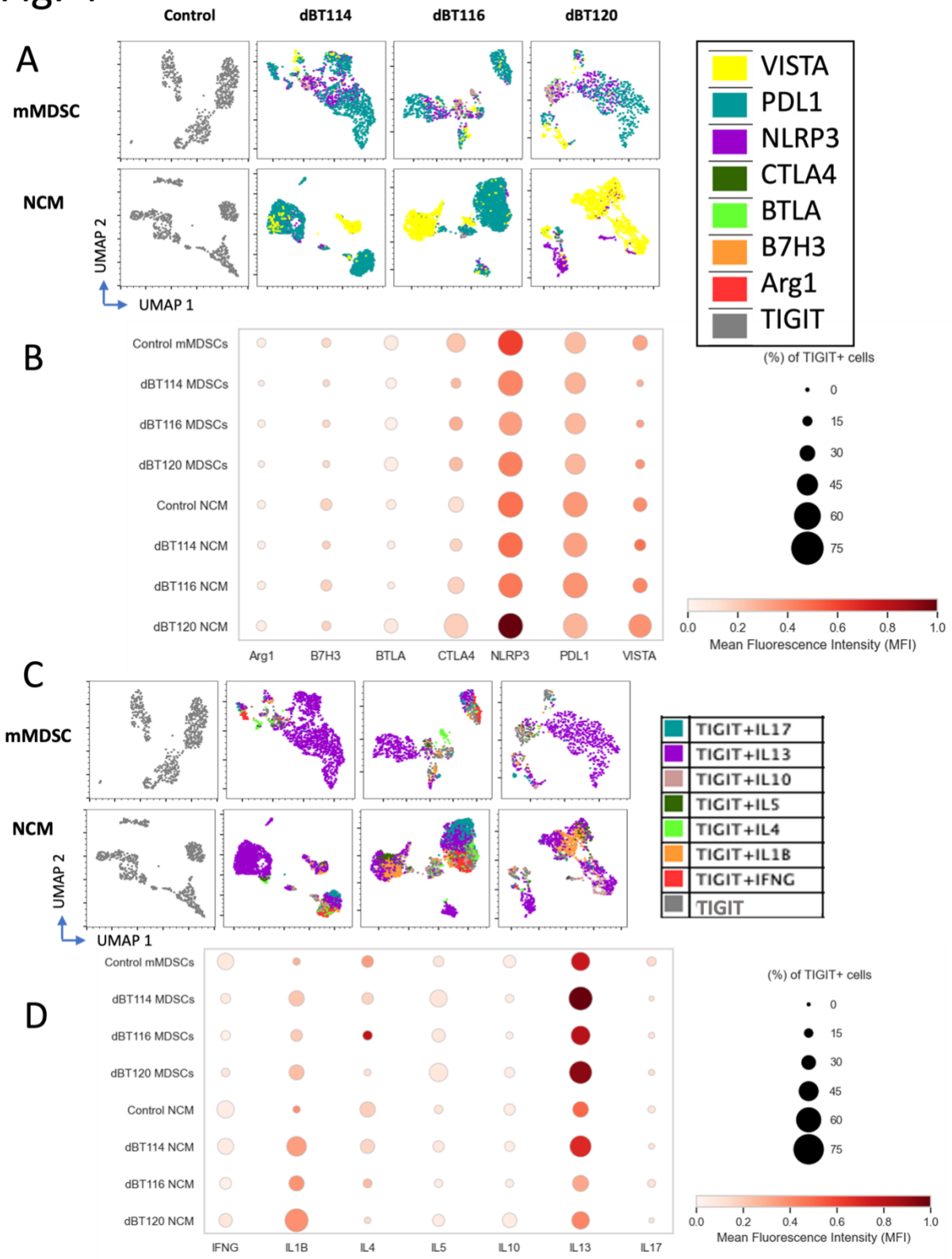
Control
dBT114
dBT116
dBT120
A
mMDSC
NCM
UMAP 2
UMAP 1
VISTA
PDL1
NLRP3
CTLA4
BTLA
B7H3
Arg1
TIGIT
B
Control mMDSCs
dBT114 MDSCs
dBT116 MDSCs
dBT120 MDSCs
Control NCM
dBT114 NCM
dBT116 NCM
dBT120 NCM
Arg1
B7H3
BTLA
CTLA4
NLRP3
PDL1
VISTA
(%) of TIGIT+ cells
0
15
30
45
60
75
0.0
0.2
0.4
0.6
0.8
1.0
Mean Fluorescence Intensity (MFI)
C
mMDSC
NCM
UMAP 2
UMAP 1
TIGIT+IL17
TIGIT+IL13
TIGIT+IL10
TIGIT+IL5
TIGIT+IL4
TIGIT+IL1B
TIGIT+IFNG
TIGIT
D
Control mMDSCs
dBT114 MDSCs
dBT116 MDSCs
dBT120 MDSCs
Control NCM
dBT114 NCM
dBT116 NCM
dBT120 NCM
IFNG
IL1B
IL4
IL5
IL10
IL13
IL17
(%) of TIGIT+ cells
0
15
30
45
60
75
0.0
0.2
0.4
0.6
0.8
1.0
Mean Fluorescence Intensity (MFI)

266

267 **Figure 4: Immune response by TIGIT$^+$ suppressive monocytes.** Isolated peripheral blood CD11b$^+$
268 monocytes were induced with TEVs in hypoxia chamber in serum free medium. After 72 hours of
269 induction, cells were processed for flow cytometric studies. Single viable CD45$^+$TIGIT cells were selected
270 for the analysis. (**A**) UMAP analysis of mMDSCs and NCM treated with control or different TEV
271 preparations (dBT114, dBT116, dBT120), highlighting the co-expression of various immune modulatory
272 molecules (VISTA, PDL1, NLRP3, CTLA4, BTLA and ARG1) within TIGIT$^+$ cell population. (**B**) Dotplot
273 depicting the percentage of cells as a factor of size of the dot expressing different immune modulatory
274 molecules within the TIGIT pockets of mMDSCs and NCMs treated with control or different EV
275 preparations. Mean fluorescence intensity (MFI) shown corresponding to the color intensity of the dots for
276 each analyte. (**C**) UMAP analysis of mMDSCs and NCM treated with control or different TEVs,
277 highlighting the expression of various cytokines (IL17, IL13, IL10, IL5, IL4, IL18, IFNγ). (**D**) Dotplot
278 depicting the percentage and MFI of TIGIT$^+$ cells co-expressing different cytokines in mMDSCs and NCM
279 treated with control or different EV preparations.

280 immunomodulatory protein hierarchy that may be leveraged to repolarize towards an
281 anti-tumor immune response.

282 TIGIT knockdown in EV-conditioned monocytes results in a pro-inflammatory 283 phenotype

284 To test if the TIGIT driven immunomodulatory hierarchy regulates the NLRP3-mediated
285 protective immune response against GBM, we next sought to determine if prevention of
286 TIGIT expression on monocytes was sufficient to 'unmask' a pro-inflammatory
287 phenotype in EV-induced immunosuppressive monocytes. Prior to EV conditioning,
288 monocytes isolated from PBMCs were treated with TIGIT-directed siRNA to knock down
289 TIGT expression. GBM-EVs were subsequently added for 72h of hypoxic co-culture as
290 described above. TIGIT knockdown demonstrated immunomodulatory reprogramming in

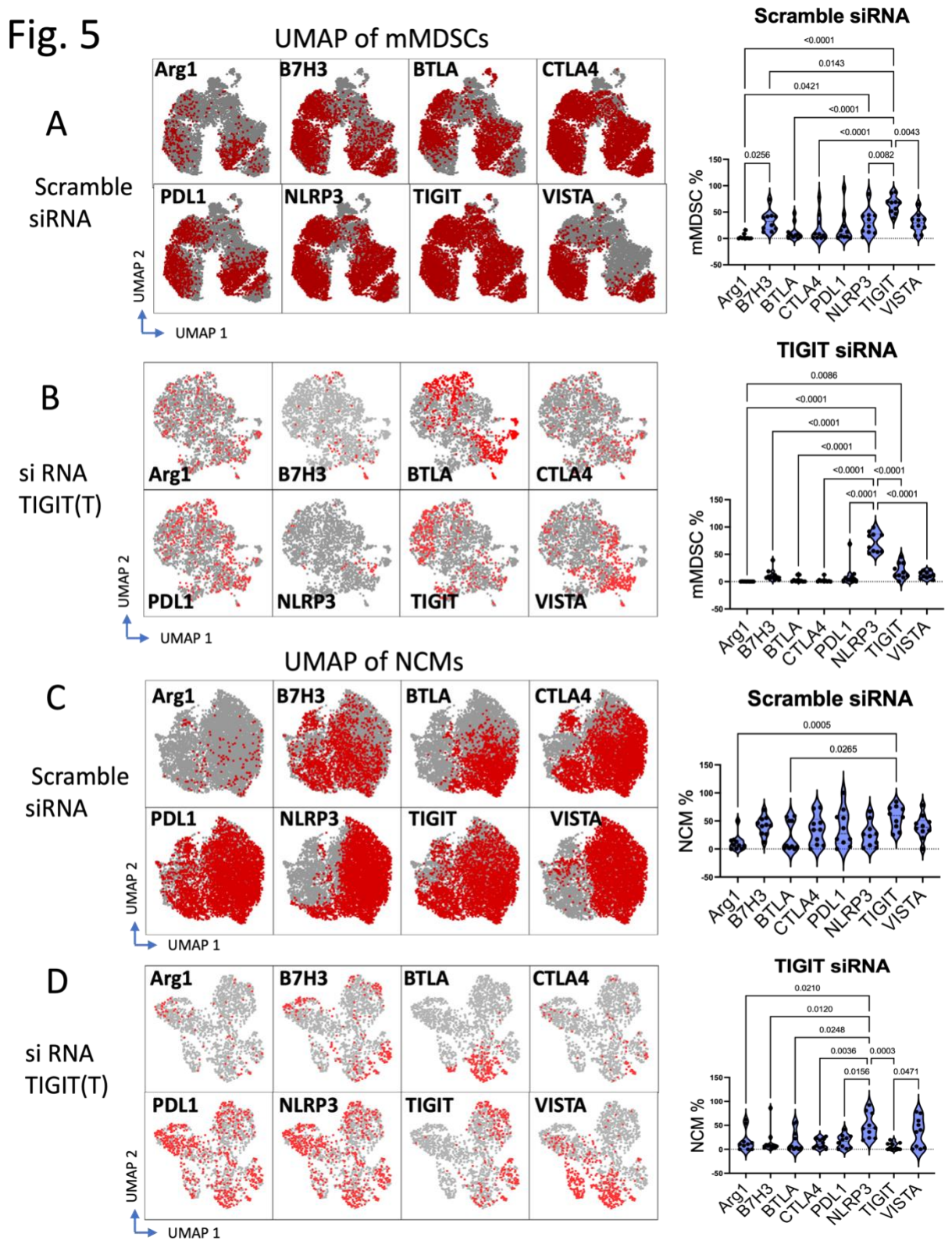

291

292 **Figure 5. Immune modulatory molecules expressing Immune suppressive monocytes post TIGIT**

293 **knockdown.** Isolated CD11b^{+} Monocytic cells from healthy peripheral blood were knockdown by
294 scramble or NLRP3-specific or TIGIT-specific siRNA and processed for flow cytometry post TEVs
295 treatment for 72 hours under hypoxia in serum free condition. (**A and B**) Uniform Manifold Approximation
296 and Projection (UMAP) plots showing the expression patterns of immune checkpoint molecules (Arg1,
297 B7H3, BTLA, CTLA4, PD-L1, NLRP3, TIGIT, and VISTA) across different clusters by mMDSC population
298 post TIGIT specific siRNA- (b) or scramble siRNA- (a) treated cells. Red color represents high expression,
299 whereas gray indicates the total cellular population of mMDSCs. Violin plots depicting the percentage of
300 mMDSCs expressing various immune modulatory molecules in TIGIT siRNA-treated and scramble
301 siRNA-treated peripheral monocytes. (**C and D**) UMAP showing the expression of the same molecules by
302 non-classical monocytes (NCM), after TIGIT siRNA-treated (d) and scramble siRNA-treated (c) peripheral
303 monocytes. Violin plots depicting the percentage of NCMs expressing various immune modulatory
304 molecules in TIGIT siRNA-treated and scramble siRNA-treated cells. Data are presented as
305 mean ± s.e.m. and were analyzed by one-way analysis of variance (ANOVA) with Tukey's multiple
306 comparisons.

307 both mMDSC and NCM immunosuppressive monocyte populations (**Fig. 5**). While
308 TIGIT knockdown in mMDSCs resulted in reduced expression of other key
309 immunomodulatory markers including B7-H3 (11.6±3.39), PD-L1 (11.04±6.59), VISTA
310 (12.3±2.05), and CTLA-4 (2.19±1.18, **Fig. 5B**) relative to scramble treated controls
311 (32.73±6, 20.52±9.4, 29.46±5.6 and 18.12±8.1 respectively, **Fig. 5A**), this effect in
312 NCMs did not reach a significant difference in any of the above mentioned immune
313 regulatory proteins (B7-H3 15.72±8.09, PD-L1 16.49±4.37, VISTA 34.82±9.7 and CTLA-
314 4 12.38±3.12, respectively) compared to scramble controls (41.55±5.19,37.04±10.35,
315 39.20±6.7 and 33.66±8.35, **Fig. 5C, D, Fig. S4**). Meanwhile, NLRP3 expressing cells
316 remained significantly elevated following TIGIT knockdown in both populations
317 (72.58±5.78 and 48.75±8.19 respectively compared to respective scrambles, 31.2±7.65
318 and 25.61 $p<0.05$, **Fig. 5B, D**).

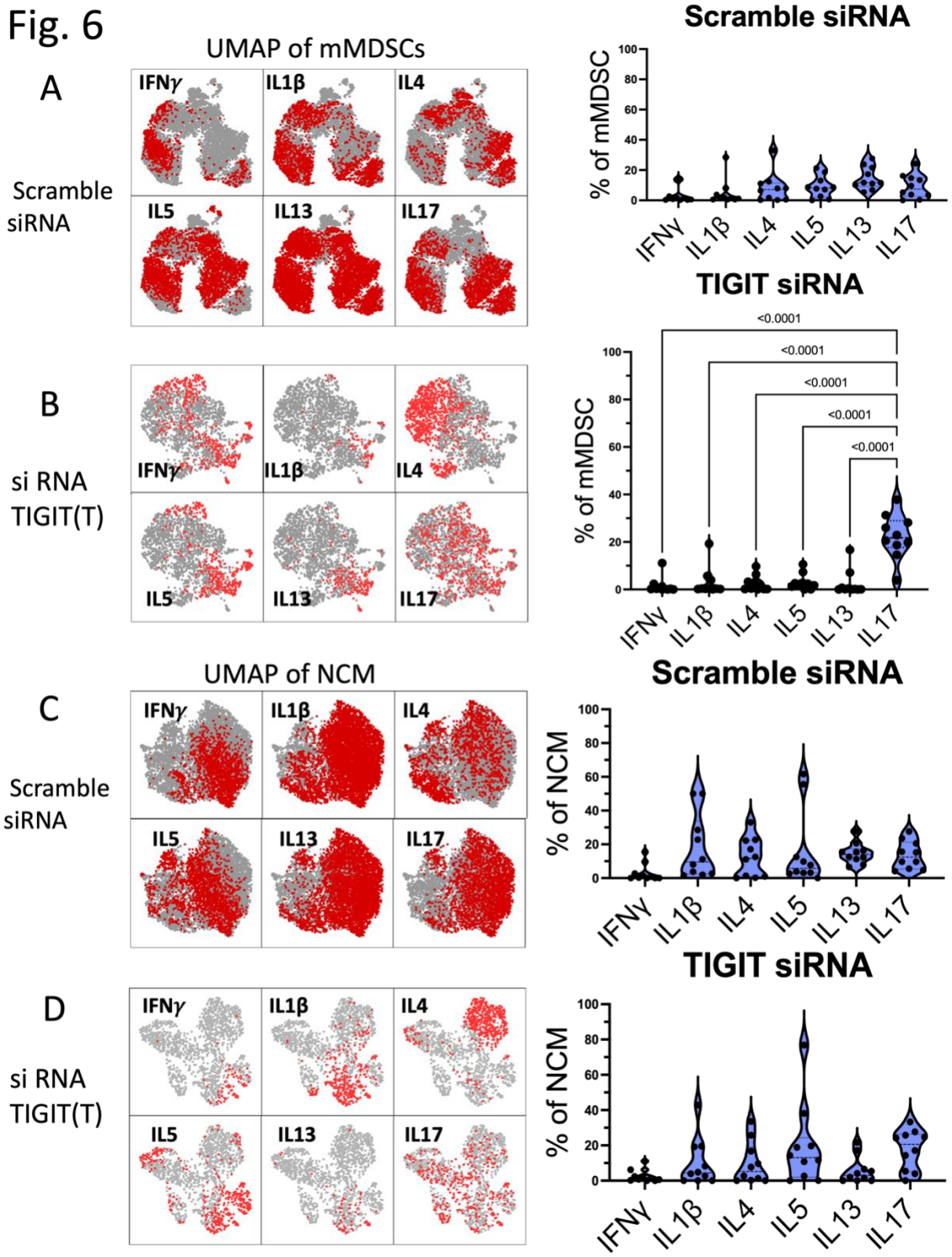

319

320 **Figure 6. Immune modulatory milieu by immune suppressive monocytes post-TIGIT knockdown.**

321 CD11b$^+$ cells isolated from healthy peripheral blood mononuclear cells (PBMCs) were knockdown by
322 TIGIT-specific or scramble siRNA under hypoxic condition in serum free medium. These healthy
323 monocytes were co-cultured with TEVs for 72 hours and processed for flow cytometry. (**A and B**) UMAP
324 plots showing the cellular distribution of mMDSCs based on their expression of various cytokines (IL17,
325 IL13, IL10, IL5, IL4, IL1β, and IFNγ) producing cells in scramble-treated (a) and TIGIT-knockdown
326 monocytes (b). Red color represents high expression, whereas gray indicates the total cellular population
327 of mMDSC. Violin plots comparing the percentage of mMDSCs expressing these cytokines between the
328 scramble-treated and TIGIT-knockdown groups. (**C and D**) UMAP showing the expression of the same
329 cytokines producing cells, (IL17, IL13, IL10, IL5, IL4, IL1β, and IFNγ) among non-classical monocytes
330 (NCM), in scramble-treated and TIGIT-knockdown groups. Violin plots comparing the percentage of
331 NCMs expressing various given cytokines between the scramble-treated and TIGIT-knockdown groups.
332 Data are presented as mean ± s.e.m. and were analyzed by one-way analysis of variance (ANOVA) with
333 Tukey's multiple comparisons.

334 We next examined the effect of TIGIT knockdown on cytokine expression in these
335 immunosuppressive monocyte populations. This revealed a marked increase in IL17-
336 expressing cells relative to scramble controls in both mMDSC and NCM populations
337 (**Fig. 6B, D**). However, this enhanced IL17 expression was significantly higher in
338 mMDSCs. Interestingly, increased IL17 expression was coupled with an attenuation of
339 IL13 expression, in TIGIT downregulated monocyte subsets, which as mentioned above
340 (**Fig. 4**) previously co-localized heavily with TIGIT$^+$ immunosuppressive monocytes (**Fig.
341 6 A, C, Fig. S5**). Interestingly, IL13 expressing cells were observed to co-expressed
342 with NLRP3$^+$ cells within the mMDSCs and NCMs (**Fig. 5** and **6**). Furthermore, IL1β
343 expressing cells also exhibited co-expression with NLRP3 in the NCM (**Fig. 5D** and **6D**).
344 Collectively, these data indicate that TIGIT-dependent IL13 may play a role in regulating
345 NLRP3-mediated inflammation.

346 **TIGIT knockdown in EV-conditioned monocytes rescues T cell proliferation in an**
347 **NLRP3-dependent manner**

348 To assess the impact of TIGIT knockdown on the immunosuppressive function of
349 immunomodulatory monocytes, we co-cultured donor-matched T cells with EV-
350 conditioned monocytes with or without siRNA-mediated TIGIT knockdown as described
351 above. Our previous work has demonstrated that EV-induced immunosuppressive
352 monocytes readily suppress T cell proliferation (*7, 10, 14*). In the present study, we
353 found that TIGIT knockdown prior to EV conditioning rescued T cell proliferation to
354 levels comparable to monocytes treated with scramble controls ($p<0.0265$, **Fig. 7A**).
355 This also resulted in reduction of the number of $IL4^+$ $CD4^+$ T cells following co-culture
356 ($p<0.025$, **Fig. 7D**).

357 Based on our earlier results demonstrating high level of NLRP3 co-expressed with
358 TIGIT cells, we wished to interrogate if this apparent rescue of TH1-type immune
359 function was dependent on NLRP3 expression. By treating PBMC-derived monocytes
360 with siRNA targeting NLRP3 and subsequently both TIGIT and NLRP3, we found that
361 NLRP3 knockdown was sufficient to eliminate the rescue of T cell proliferation observed
362 following TIGIT knockdown (**Fig. 7A**). NLRP3 and TIGIT double knockdown also
363 eliminated the increase in $CD4^+$ T cells observed following TIGIT knockdown (**Fig. 7B**)
364 as well as the reduction in IL-4+ CD4+ T cells observed with TIGIT knockdown alone.
365 Although there was not much effect on IFNγ level (**Fig. 7C**), however, the ratio of
366 IFNγ/IL-4+ T cells increased significantly with TIGIT knockdown in monocytes alone
367 (**Fig. 7E**), an effect that was eliminated with NLRP3 knockdown.

Fig. 7

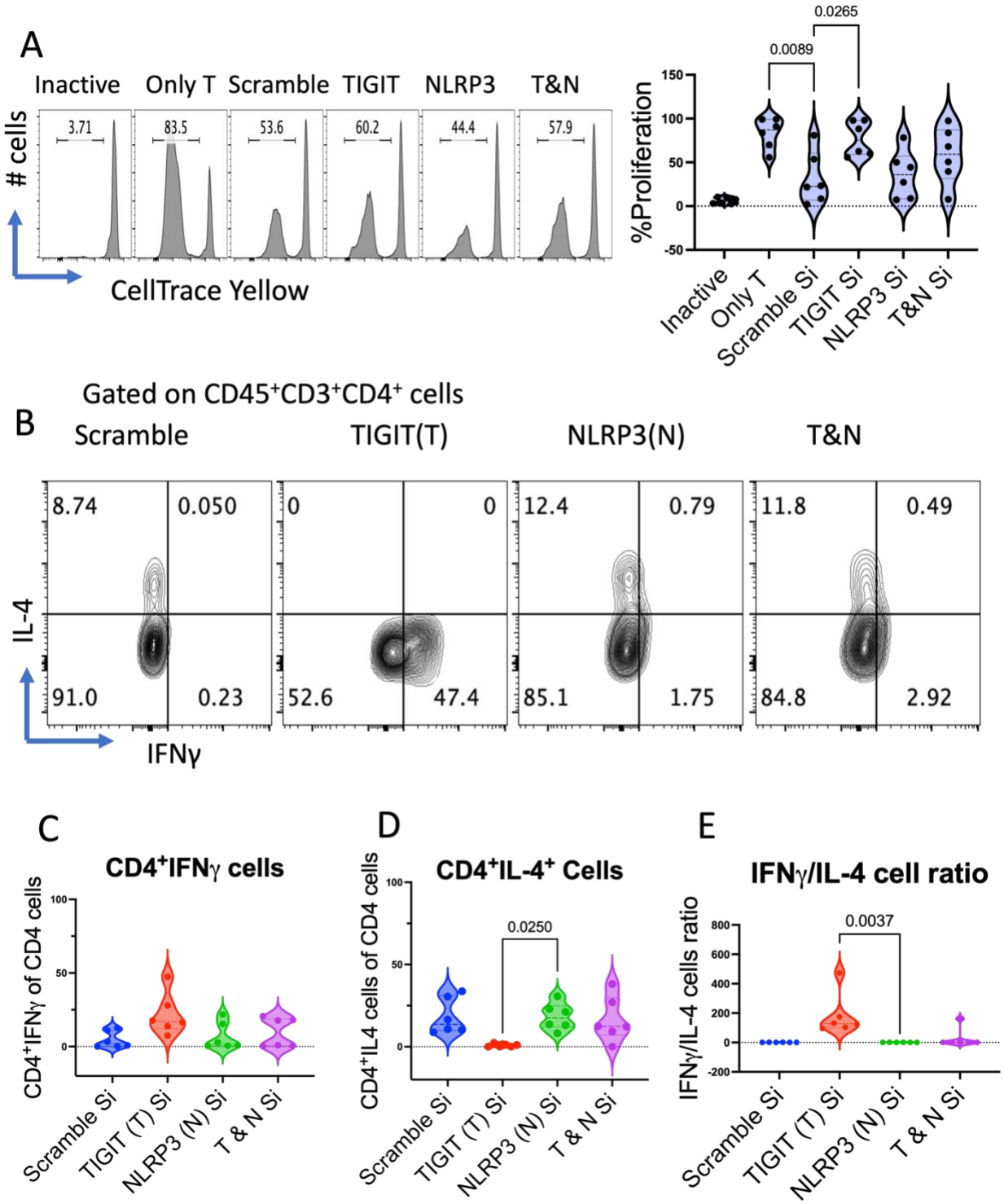

Figure 7. Effect of TIGIT knockdown on T Cell Proliferation in the Presence of TEV-Induced MDSCs.

371 CD11b+ and CD3+ cells were isolated from healthy volunteer peripheral blood monocytes. CD11b cells
372 were conditioned with TIGIT and NLRP3-specific siRNA in serum-free medium followed by priming with
373 TEVs for under hypoxic conditions (1%) for 72 hours. Then, CD11b and T cells (T cells stained with cell
374 trace yellow dye) were co-cultured for another 72 hours in RPMI-1640 medium with 10% serum at 37°C in
375 5% CO2. Finally, cells were processed for flow cytometry. (**A**) Representative flow cytometry plots and
376 corresponding bar graphs showing $CD3^+$ T cell proliferation (Cell Trace Yellow) in the absence of T cell
377 activator, CD3/CD28 Dynbeads (inactive group), when T cells were cultured without conditioned
378 monocytes Only T cell group), scramble treated group, TIGIT specific siRNA treated group (TIGIT),
379 NLRP3 specific siRNA treated group (NLRP3) and both TIGIT along with NLRP3 siRNA treated group
380 (T&N). (**B**) Representative flow cytometry plots showing IFNγ and IL-4 producing CD4+ T cells in $CD3^+$ T
381 cells and $CD11b^+$ monocytes co-culture conditions, post scramble, TIGIT and/or NLRP3 knockdown. (**C**)
382 IFNγ producing CD4+ T cells in the above-mentioned co-culture conditions in the given treatment groups.
383 (**D**) IL-4 producing CD4+ T cells in $CD3^+$ T cells and $CD11b^+$ monocytes co-culture conditions, post
384 scramble, TIGIT and/or NLRP3 knockdown. (**E**) Ratio of IFNγ producing $CD4^+$ T cells and IL-4 producing
385 $CD4^+$ T cells in the given co-culture conditions. Data are presented as mean ± s.e.m. and were analyzed
386 by one-way analysis of variance (ANOVA) with Tukey's multiple comparisons.

387 **Discussion**

388 Anti-cancer immunotherapy, including immune checkpoint blockade, has revolutionized
389 the treatment of several solid tumors in recent years (*22, 23*). Metastatic melanoma,
390 which once carried a prognosis comparable to GBM, has seen a revolution in outcomes
391 with immune checkpoint therapy (*3, 24*). Several clinical trials have explored these
392 treatments in GBM, but the results have been disappointing (*5, 25, 26*). Several
393 mechanisms for these failures have been implicated, including the mutational burden of
394 GBM, the immune specialization of the central nervous system, but the profound
395 immune derangement found in GBM patients is a long-described and under explored
396 phenomena (*7, 27-29*). The mechanisms of systemic immune suppression generated by

397 a localized disease such as GBM remains an area of active study, but induction of distal
398 effector signals, including EVs and immunosuppressive myeloid cells, are potent
399 avenues by which such effects could be achieved.

400 Work by our group and others has contributed to a growing body of evidence that
401 myeloid cells in the GBM microenvironment are major intermediaries of tumor-mediated
402 immune suppression, and that GBM-EVs are an effective means of inducing the
403 formation of immunosuppressive myeloid cells (*10, 17, 30*). These myeloid cells are a
404 highly heterogenous milieu, comprised of as many as 14 subtypes of cells as recently
405 described (*8*), and the relative import of different immunosuppressive myeloid cell
406 populations to the overall milieu is an open question. In our study, we focused on
407 mMDSCs and NCMs as exemplar immunosuppressive monocyte populations, as our *in*
408 *situ* tumor microenvironment data demonstrates a robust presence in the GBM
409 microenvironment and previous work has demonstrated that these populations are
410 modifiable by GBM-EVs (*10, 14, 30*). A central question to unlocking the complexity of
411 the tumor-immune microenvironment is understanding the relative import and/or
412 functional redundancy of these immunosuppressive cell populations, in order to define
413 the critical therapeutic targets in order to effectively repolarize the tumor
414 microenvironment to allow for anti-tumor immunity.

415 In the present study, we were surprised to find broad TIGIT expression across a large
416 swath of cells in the GBM microenvironment, including immunosuppressive myeloid
417 cells such as MDSCs and NCMs. Further, TCGA data indicated an association of TIGIT
418 expression with reduced patient survival, indicating a potential role for TIGIT expression
419 in disease severity. TIGIT has been classically described as a T cell exhaustion marker

420 (*31, 32*), but some reports do describe a role for TIGIT expression in myeloid cells (*33-*
421 *35*), including a study that indicated a correlation with prognosis in GBM patients (*20*).
422 Anti-TIGIT antibodies have had some success in clinical trials as an anti-cancer
423 immunotherapy (*36*), but have yet to show benefit in GBM treatment (*37*).

424 We found in our study that TIGIT expression correlated with several pro-inflammatory
425 markers in otherwise phenotypically immunosuppressive myeloid cells, with particularly
426 strong co-expression of TIGIT and NLRP3. NLRP3 is typically associated with the
427 inflammasome and the production of pro-inflammatory cytokines such as IL-1B (*38-40*).
428 The role of NLRP3 in cancer is more controversial, with many studies pointing to an
429 immunosuppressive role, while others suggest a beneficial role (*41, 42*). The larger
430 tumor-immune context may well provide an explanation for these mixed findings.
431 Indeed, we found that knockdown of TIGIT resulted in a pro-inflammatory polarization of
432 mMDSCs and NCMs, and that this effect was lost upon concomitant knockdown of
433 NLRP3. These results are suggestive of a hierarchical arrangement of
434 immunomodulatory signals in myeloid cells in the GBM tumor microenvironment.
435 Inhibition of a specific immune checkpoint may be insufficient to eliminate the
436 immunosuppressive effects of these cells given the presence of redundant signals, but
437 prevention certain of these signals may signify a globally immunosuppressive
438 phenotype. Prevention of the expression of certain hierarchically important signals, such
439 as TIGIT in the present study, may be sufficient to repolarize these cells to a pro-
440 inflammatory phenotype, which could have major implications for reversal of tumor-
441 mediated immune suppression.

442 **Materials and methods**

443 **Study design**

444 To identify potential therapeutic targets within the glioblastoma (GBM) tumor
445 microenvironment, we analyzed the immune phenotype of myeloid cells obtained from
446 surgical resection specimens using ultrasonic aspirates. This direct approach allowed
447 for the identification of immunomodulatory markers across diverse myeloid cell
448 populations. These findings were then validated using an *in vitro* model of
449 immunosuppressive monocyte induction, where healthy monocytes were exposed to
450 GBM-derived extracellular vesicles (EVs) from patient-derived cell lines. TIGIT
451 knockdown studies were then performed to interrogate its import on the
452 immunosuppressive polarization of myeloid cells. Subsequent donor-matched T cell
453 proliferation studies were then performed as a functional measure of
454 immunosuppressive activity.

455 **Patient cohort and sample processing**

456 Patients with glioblastoma (GBM) were diagnosed via standard magnetic resonance
457 imaging (MRI) of the brain. Written informed consent was obtained from all surgical
458 candidates prior to surgery, in accordance with the protocol approved by the Institutional
459 Review Board of Montefiore Medical Center (IRB# 2022-14518). Study patients (n= 14)
460 underwent surgery with the goal of maximum, safe resection. The diagnosis of GBM
461 was confirmed through histological review by a trained neuropahtoligst, and by
462 subsequent genetic testing. Patients received standard oncological treatment with
463 temozolamide and fractioned radiotherapy and close clinical follow-up according to
464 national guidelines at Montefiore Medical Center, Bronx, NY.

465 During surgery, tumor specimens were collected, and ultrasonic aspirates were
466 immediately placed on ice for processing. Fresh tumor tissue was mechanically
467 dissociated using a scalpel and then enzymatically digested with TrypLE Express
468 (Gibco, 12605010) at 37°C for 10 minutes. The resulting cell suspension was filtered
469 through 40 µm nylon mesh, treated with red blood cell lysis buffer (BioLegend, 420301),
470 and washed with phosphate-buffered saline (PBS). Single-cell suspensions were then
471 prepared for flow cytometry analysis.

472 **Cell Culture**

473 Primary glioblastoma (GBM) cell lines, designated dBT114, dBT116, and dBT120, were
474 initially established as brain tumor stem cell neurospheres in serum-free, HEPES-
475 modified DMEM/F12 medium supplemented with EGF, FGF, and N2, as previously
476 described (*43*). Subsequently, these cell lines were adapted to grow as adherent
477 monolayers in HEPES-modified EmbryoMax DMEM/F12 medium (DF-042-B, Millipore,
478 Burlington, MA) containing 1% penicillin/streptomycin and 10% fetal calf serum. Cells
479 were maintained in T75 flasks at 37°C with 5% CO2 in a humidified incubator, as
480 previously described (*10*). The cells were grown as an adherent monolayer and
481 passaged when confluency was around 90%. Early passages within 10 or lower were
482 used for the study.

483 **EV Isolation and protein estimation**

484 For isolation of EVs, dBT114, dBT116 and dBT120 cells were transferred to serum-free
485 neurosphere culture, DMEM: F12 medium containing EGF and FGF growth factors in
486 5% CO_2 incubator. After 72 hrs, as described earlier (*43*), cultured supernatants were

487 collected in 50 ml centrifuge tubes and centrifuged at 1900 *g* for 10 min at room
488 temperature. Then supernatants were transferred to 14 ml propylene Ultracentrifuge
489 tubes, 14 X 95 mm (Cat# 331374, Beckman Coulter, Brea, CA) and centrifuged at
490 24000 rpm for 16 hrs at 4°C on Optima XE-90 ultracentrifuge (Beckman Coulter, Brea,
491 CA). After centrifugation, a small, thin transparent pellet deposited at the bottom of the
492 tube were carefully resuspended in the 200 µl of the same neurosphere medium.
493 Resuspended EVs were collected in a cryovial, and protein concentration was
494 calculated by modified Pierce Rapid Gold BCA Protein Assay Kit (A53226, Thermo
495 Fisher, Waltham, MA) according to manufacturer's method and the reading was
496 acquired by Infinite 200Pro plate reader (Tecan, Mannedorf, Switzerland) using software
497 Tecan I-Control (version 2.0). The isolated EVs were stored at -80°C freezer until used.

498 **EV characterization**

499 EVs were characterized using the NanoSight Nanotracker system (ZetaView, Particle
500 Metrix GmbH). Freshly isolated EVs were diluted 1000-fold with filtered (40 nm syringe
501 filter) phosphate-buffered saline to achieve a particle concentration suitable for analysis
502 and to remove larger particles or aggregates. One µL of the diluted EV solution was
503 loaded into the capillary system of the ZetaView, where a laser illuminated individual
504 EVs, and their Brownian motion was tracked by a camera. The ZetaView software
505 calculated the size of each EV using the Stokes-Einstein equation and generated a
506 histogram and images showing the shape, size distribution and concentration of EVs in
507 the sample.

508 **Peripheral blood mononuclear cells (PBMC) Isolation**

509 Human blood samples were obtained from the New York Blood Center from healthy
510 donors (n=10). Either heparin or EDTA was used as an anticoagulant. Blood samples
511 were delivered at room temperature (~24°C) and processed immediately after the
512 delivery. All subsequent steps were performed at room temperature. PBMCs were
513 isolated from whole blood using standard density gradient centrifugation with Ficoll-
514 Paque PLUS (17-5442-03, density 1.077 ± 0.001 g/ml, GE Healthcare, Chicago, IL) as
515 described earlier (*30*). Briefly blood was diluted 1:1 with 1X PBS and mixed gently.
516 Ficoll-Paque™ Premium was added to the bottom of a sterile 50 ml centrifuge tube. The
517 diluted blood was carefully layered on top of the Ficoll-Paque, maintaining a clear
518 interface between the two layers. The tube was centrifuged at 500g for 30 minutes
519 without brake. PBMCs were collected from the interface between the plasma and Ficoll
520 layers using a sterile transfer pipette. The collected PBMCs were washed with PBS to
521 remove any residual Ficoll or other contaminants and resuspended in PBS + 2% FBS.
522 Cells were counted using the trypan blue exclusion method on Countess 3 (Invitrogen,
523 Waltham, MA).

524 **Isolation of monocytes**

525 Monocytes were positively selected from healthy donor PBMCs, using CD11b
526 MicroBeads (130-049-601, Miltenyi Biotec, Bergisch Gladbach, Germany). Briefly, 5 µL
527 of CD11b MicroBeads were added per 10^7 total cells, and the mixture was incubated for
528 30 minutes at room temperature. Cells were then washed twice with PBS + 2% FBS
529 and resuspended in PBS + 2% FBS. The cell suspension was applied to an LS column
530 placed in a magnetic field of a MACS Separator. Unlabeled cells were collected as the
531 flow-through fraction. The column was then removed from the magnetic field, and

532 labeled monocytes were eluted by flushing the column with PBS + 2% FBS. The purity
533 of the isolated monocytes was assessed by flow cytometry using anti-CD45 and anti-
534 CD11b antibodies.

535 **Monocyte Culture and EV Treatment**

536 Purified human monocytes were cultured in L-glutamine and HEPES-modified DMEM
537 medium supplemented with 1% penicillin/streptomycin under hypoxic conditions (1%
538 O2). Cells were seeded at a density of 1 million cells per well in a 96-well plate.
539 Monocytes were treated with purified extracellular vesicles (EVs) (20 µg/well) isolated
540 from various glioblastoma cell lines (dBT114, dBT116 and dBT120). Cells were cultured
541 for 72 hours under hypoxic conditions.

542 **Cell Preparation and Staining for flow cytometry**

543 Cultured and EV-stimulated monocytes were washed twice with PBS only and
544 resuspended in 50 µl of PBS and processed for flow cytometric study as described
545 earlier (Asad et al. Front Immunol, 2019). Briefly, cells were stained with LIVE/DEAD
546 Fixable Blue Dead Cell Stain (Thermo Fisher Scientific) for 30 minutes at room
547 temperature in the dark. Following staining, cells were washed twice with FACS buffer
548 (containing 2% human serum) and resuspended in 50 µl of FACS buffer. To block non-
549 specific binding, cells were incubated with Fc blocking solution for 20 minutes at room
550 temperature. Subsequently, cells were washed twice with FACS buffer and resuspended
551 in 50 µl of staining buffer containing a cocktail of fluorochrome-conjugated antibodies
552 specific for surface markers of interest. Cells were incubated for 60 minutes at 4°C in
553 the dark. Following surface staining, cells were washed twice with FACS buffer and

554 resuspended in 50 µl of FACS buffer containing 2% human serum. Cells were fixed and
555 permeabilized using Cytofix/Cytoperm solution (BD Biosciences, San Jose, CA) for 20
556 minutes at 4°C. Cells were then washed twice with permeabilization buffer and
557 incubated with 50 µl cocktail of fluorochrome-conjugated antibodies specific for
558 intracellular markers of interest for overnight (12-14 hrs) at 4°C in the dark. After
559 incubation, cells were washed twice with permeabilization buffer, resuspended in 200 µl
560 of FACS buffer, and filtered through a 70-micron nylon mesh to remove cell clumps.
561 Finally, samples were acquired on a Cytek Aurora 5 laser flow cytometer and analyzed
562 using FlowJo software.

563 **Isolation of CD3+ T cells and T cell proliferation assay**

564 PBMCs were isolated from healthy human donors using standard density gradient
565 centrifugation, as described above. CD3+ T cells were then purified from PBMCs via
566 magnetic cell sorting using a commercially available kit (130-050-101, Miltenyi Biotec,
567 Bergisch Gladbach, Germany), following a similar procedure to the previously described
568 CD11b isolation. Isolated CD3+ T cells were cultured at a density of 1 x 10^7 cells/ml in
569 RPMI-1640 medium supplemented with 1% penicillin-streptomycin and 10% fetal bovine
570 serum for 3 days at 37°C in 5% CO2. CD3+ T cells were labeled with CellTrace Yellow
571 according to the manufacturer's instructions. CD11b+ monocytes were conditioned with
572 extracellular vesicles (EVs) derived from primed CD11b+ monocytes. Donor-matched
573 autologous labeled CD3+ T cells were co-cultured with EV-conditioned CD11b+
574 monocytes at a 1:1 ratio (1 x 10^6 cells each) in RPMI-1640 medium supplemented with
575 1% penicillin-streptomycin and 10% fetal bovine serum in the presence of aCD3/aCD28
576 DynaBeads (11131D Thermo Fisher, Waltham, MA) for 5 days at 37°C in 5% CO2. After

577 5 days of co-culture, cells were harvested and processed for flow cytometry analysis. A
578 subset of conditioned cells was used for cellular proliferation assays. Cells were labeled
579 with CFSE or Yellow Fluorescent Dye and analyzed by flow cytometry using a Cytek
580 Aurora flow cytometer. Another subset of conditioned cells was used for flow cytometry
581 analysis using a Cytek Aurora flow cytometer to assess changes in cell surface markers
582 or intracellular signaling pathways.

583 **T Cell Suppression/Proliferation Assay**

584 PBMCs were isolated from healthy human donors, and CD3+ T cells and CD11b+
585 monocytes were purified using magnetic sorting, as described above. CD3+ T cells
586 were cultured at a density of 10^7 cells/mL in RPMI-1640 medium supplemented with
587 10% fetal bovine serum (FBS; Genesee, El Cajon, CA) and 1% penicillin-streptomycin.
588 Cells were maintained at 37°C in a humidified incubator with 5% CO_2 for 5 days prior to
589 co-culture with extracellular vesicle (EV)-primed CD11b+ monocytes.

590 **CD11b+ Monocyte Conditioning and EV Stimulation**

591 Purified CD11b+ monocytes (10^6 cells/well) were plated in a 96-well plate in 100 µL of
592 serum-free medium (Dharmacon, Lafayette, CO) containing 1% penicillin-streptomycin
593 and transfected with Accell small interfering RNA (siRNA; Dharmacon, Lafayette, CO) at
594 a final concentration of 1 µM. Cells were incubated under normoxic conditions (37°C,
595 5% CO_2) for 48 hours. Following incubation, CD11b+ monocytes were stimulated with
596 20 µg of tumor-derived extracellular vesicles (TEVs) and cultured for an additional 72
597 hours under hypoxic conditions (1% O_2, 5% CO_2, 37°C).

598 **T Cell Labeling and Co-Culture**

599 Following the 72-hour incubation, CD3+ T cells were washed with phosphate-buffered
600 saline (PBS) and labeled with CellTrace Yellow (Thermo Fisher Scientific, Waltham, MA)
601 according to the manufacturer's instructions. Labeled CD3+ T cells (10^6 cells) were co-
602 cultured at a 1:1 ratio with EV-primed CD11b+ monocytes in RPMI-1640 medium
603 supplemented with 10% FBS and 1% penicillin-streptomycin. Cells were stimulated
604 using pre-washed αCD3/αCD28 DynaBeads (11131D, Thermo Fisher Scientific,
605 Waltham, MA) at a concentration of 20 μL beads per million cells and incubated under
606 normoxic conditions (5% CO_2, 37°C) for 3 days.

607 **Flow Cytometry and Proliferation Assay**

608 Following a 3-day co-culture period, cells were harvested from the 96-well U-bottom
609 plates and prepared for flow cytometry staining using an optimized laboratory protocol.
610 Unbound DynaBeads were removed by placing the culture tube on a magnet for 2
611 minutes, after which the supernatant containing cells was transferred to a fresh tube. T
612 cell proliferation was assessed via CellTrace Yellow dilution, and additional
613 multiparametric immunophenotypic analyses were performed using flow cytometry.

614 **Immunofluorescence Staining of Monocytes**

615 Human monocytes were cultured in an 8-well chamber slide at a density of 1×10^6 cells
616 per well and allowed to adhere under standard conditions (37°C, 5% CO_2). After
617 adherence, the culture medium was aspirated, and cells were gently rinsed with
618 phosphate-buffered saline (PBS). Fixation was performed using 4% paraformaldehyde
619 (PFA) in PBS for 15 minutes at room temperature (RT), followed by three washes with

620 PBS (5 minutes each). Cells were permeabilized using 0.1% Triton X-100 in PBS for 10
621 minutes at RT and washed three times with PBS. To block non-specific binding, cells
622 were incubated in blocking buffer (5% bovine serum albumin [BSA] in PBS) for 1 hour at
623 RT in a humidified chamber. Cells were incubated with the primary antibody diluted in
624 blocking buffer at the recommended concentration overnight at 4°C in a humidified
625 chamber. After incubation, cells were washed three times with PBS (5 minutes each). A
626 fluorophore-conjugated secondary antibody was diluted in blocking buffer and applied to
627 the cells for 1 hour at RT in the dark. Unbound antibody was removed by washing three
628 times with PBS (5 minutes each). Cells were incubated with 1 μg/mL DAPI in PBS for 5
629 minutes at RT and subsequently washed three times with PBS. The chamber walls were
630 carefully removed, and a drop of mounting medium was applied to each well. Coverslips
631 were placed gently to avoid bubble formation. Slides were allowed to set for at least 30
632 minutes at RT in the dark before imaging. Immunofluorescence was visualized using a
633 fluorescence microscope equipped with appropriate filter sets.

634 **Western blotting**

635 Monocytes, cultured with or without EVs stimulation were harvested and washed with
636 ice cold PBS twice. Cells were then lysed in RIPA buffer supplemented with protease
637 and phosphatase inhibitors and incubated on ice for 30 min with intermittent vortexing.
638 Lysates were centrifuged at 12,000 × g for 7 min at 4°C, and the supernatant was
639 collected. Protein concentration was determined using a Pierce Rapid Gold BCA Protein
640 Assay Kit (A53226, Thermo Fisher, Waltham, MA) according to manufacturer's
641 instructions and the reading was acquired by Infinite 200Pro plate reader (Tecan,
642 Mannedorf, Switzerland) using software Tecan I-Control (version 2.0). Equal amounts of

643 protein (20–40 µg) were resolved on a 10–12% SDS-PAGE gel at 100 V until the dye
644 front reached the bottom. Proteins were transferred to a PVDF or nitrocellulose
645 membrane using iBLOT3 (Invitrogen, Waltham, MA), a dry transfer system. Membranes
646 were blocked with 5% bovine serum albumin (BSA) or 5% nonfat milk in Tris-buffered
647 saline with Tween 20 (TBST) for 1 hour at room temperature. The membranes were
648 incubated overnight at 4°C with anti-TIGIT primary antibody PA5-121546, Invitrogen,
649 Waltham, MA) followed by three washes with TBST (5 min each). Antibodies against
650 HSP90 (Thermo Fisher, Waltham, MA) were used as control housekeeping gene. HRP-
651 conjugated secondary antibody was applied for 1 hour at RT, followed by three
652 additional washes with TBST. Proteins were detected using an enhanced
653 chemiluminescence (ECL) reagent, and signals were visualized using the
654 chemiluminescence imaging system.

655 **Statistics**

656 For statistical analysis, GraphPad Prism V.10.0 software (La Jolla, CA) was used to
657 graph the data and perform necessary calculations. Statistical comparisons were
658 primarily conducted using one-way analysis of variance (ANOVA) with Tukey's multiple
659 comparisons. Data are presented as mean ± S.E.M. and a p value threshold of <0.05
660 was set for determining statistical significance across all experiments. In the summary
661 dot plots or violin plots, each dot represent individual human value. The p values and
662 S.E.M are indicated on these plots through error bars.

663 **Supplementary Materials**

664 The PDF file includes:

Figs. S1 to S5

Tables S1 to S2

Funding: This work was supported by the Neurosurgery Research & Education Foundation through the B*CURED & NREF Young Clinician Investigator Award, as well as intramural K12 funding through the Institute for Clinical and Translational Research and the NCI Paul Calabresi Career Development Award (1K12CA279871).

Author contributions: M.A. and B.T.H. conceptualized, designed the experiments and wrote the manuscript. M.A., J.I. and Minori Aoki performed the experiments. C.C., P.L. and E.E. provided the patient samples. M.A. and J.I. conducted data analysis. S.M. help in preparing dot plot in figure 4. E.E., C.G. and X.Z. provided important advice. I.F.P. provided the GBM cell lines. B.T.H. acquired funding and directed the research.

Competing interests: The authors declare that they have no competing interest.

Data and materials availability: All data associated with this study are present in the paper or the Supplementary Materials.

References

1. R. Stupp *et al.*, Radiotherapy plus concomitant and adjuvant temozolomide for glioblastoma. *N Engl J Med* **352**, 987-996 (2005).
2. L. Marenco-Hillembrand *et al.*, Trends in glioblastoma: outcomes over time and type of intervention: a systematic evidence based analysis. *J Neurooncol* **147**, 297-307 (2020).
3. J. S. Weber *et al.*, Nivolumab versus chemotherapy in patients with advanced melanoma who progressed after anti-CTLA-4 treatment (CheckMate 037): a randomised, controlled, open-label, phase 3 trial. *Lancet Oncol* **16**, 375-384 (2015).

689 4. R. S. Herbst *et al.*, Pembrolizumab versus docetaxel for previously treated, PD-L1-
690 positive, advanced non-small-cell lung cancer (KEYNOTE-010): a randomised
691 controlled trial. *Lancet* **387**, 1540-1550 (2016).
692 5. J. F. Inocencio *et al.*, Immune checkpoint pathways in glioblastoma: a diverse and
693 evolving landscape. *Front Immunol* **15**, 1424396 (2024).
694 6. C. M. Jackson, J. Choi, M. Lim, Mechanisms of immunotherapy resistance: lessons
695 from glioblastoma. *Nat Immunol* **20**, 1100-1109 (2019).
696 7. B. T. Himes *et al.*, Immunosuppression in Glioblastoma: Current Understanding and
697 Therapeutic Implications. *Front Oncol* **11**, 770561 (2021).
698 8. C. Jackson *et al.*, Distinct myeloid-derived suppressor cell populations in human
699 glioblastoma. *Science* **387**, eabm5214 (2025).
700 9. S. Ostrand-Rosenberg, Myeloid derived-suppressor cells: their role in cancer and
701 obesity. *Curr Opin Immunol* **51**, 68-75 (2018).
702 10. B. T. Himes *et al.*, The role of extracellular vesicles and PD-L1 in glioblastoma-
703 mediated immunosuppressive monocyte induction. *Neuro Oncol* **22**, 967-978
704 (2020).
705 11. J. P. Antonios *et al.*, Immunosuppressive tumor-infiltrating myeloid cells mediate
706 adaptive immune resistance via a PD-1/PD-L1 mechanism in glioblastoma. *Neuro*
707 *Oncol* **19**, 796-807 (2017).
708 12. Y. Mi *et al.*, The Emerging Role of Myeloid-Derived Suppressor Cells in the Glioma
709 Immune Suppressive Microenvironment. *Front Immunol* **11**, 737 (2020).
710 13. M. P. Gustafson *et al.*, Systemic immune suppression in glioblastoma: the interplay
711 between CD14+HLA-DRlo/neg monocytes, tumor factors, and dexamethasone.
712 *Neuro Oncol* **12**, 631-644 (2010).
713 14. M. Y. Jung *et al.*, Superinduction of immunosuppressive glioblastoma extracellular
714 vesicles by IFN-gamma through PD-L1 and IDO1. *Neurooncol Adv* **4**, vdac017
715 (2022).
716 15. F. L. Ricklefs *et al.*, Immune evasion mediated by PD-L1 on glioblastoma-derived
717 extracellular vesicles. *Sci Adv* **4**, eaar2766 (2018).
718 16. E. I. Buzas, The roles of extracellular vesicles in the immune system. *Nat Rev*
719 *Immunol* **23**, 236-250 (2023).
720 17. N. Ludwig *et al.*, Characterization of systemic immunosuppression by IDH mutant
721 glioma small extracellular vesicles. *Neuro Oncol* **24**, 197-209 (2022).
722 18. Y. Kong *et al.*, T-Cell Immunoglobulin and ITIM Domain (TIGIT) Associates with CD8+
723 T-Cell Exhaustion and Poor Clinical Outcome in AML Patients. *Clin Cancer Res* **22**,
724 3057-3066 (2016).
725 19. L. Wu *et al.*, Blockade of TIGIT/CD155 Signaling Reverses T-cell Exhaustion and
726 Enhances Antitumor Capability in Head and Neck Squamous Cell Carcinoma.
727 *Cancer Immunol Res* **7**, 1700-1713 (2019).
728 20. I. Raphael *et al.*, TIGIT and PD-1 Immune Checkpoint Pathways Are Associated With
729 Patient Outcome and Anti-Tumor Immunity in Glioblastoma. *Front Immunol* **12**,
730 637146 (2021).
731 21. J. C. Rodrigues *et al.*, Normal human monocytes exposed to glioma cells acquire
732 myeloid-derived suppressor cell-like properties. *Neuro Oncol* **12**, 351-365 (2010).

733 22. M. A. Postow, M. K. Callahan, J. D. Wolchok, Immune Checkpoint Blockade in
734 Cancer Therapy. *J Clin Oncol* **33**, 1974-1982 (2015).
735 23. C. H. June, R. S. O'Connor, O. U. Kawalekar, S. Ghassemi, M. C. Milone, CAR T cell
736 immunotherapy for human cancer. *Science* **359**, 1361-1365 (2018).
737 24. A. Hauschild *et al.*, Dabrafenib in BRAF-mutated metastatic melanoma: a
738 multicentre, open-label, phase 3 randomised controlled trial. *Lancet* **380**, 358-365
739 (2012).
740 25. P. Y. Wen *et al.*, Glioblastoma in adults: a Society for Neuro-Oncology (SNO) and
741 European Society of Neuro-Oncology (EANO) consensus review on current
742 management and future directions. *Neuro Oncol* **22**, 1073-1113 (2020).
743 26. H. Y. Chan, J. Choi, C. Jackson, M. Lim, Combination immunotherapy strategies for
744 glioblastoma. *J Neurooncol* **151**, 375-391 (2021).
745 27. P. E. Fecci *et al.*, Increased regulatory T-cell fraction amidst a diminished CD4
746 compartment explains cellular immune defects in patients with malignant glioma.
747 *Cancer Res* **66**, 3294-3302 (2006).
748 28. C. A. Crane, B. J. Ahn, S. J. Han, A. T. Parsa, Soluble factors secreted by glioblastoma
749 cell lines facilitate recruitment, survival, and expansion of regulatory T cells:
750 implications for immunotherapy. *Neuro Oncol* **14**, 584-595 (2012).
751 29. K. Ayasoufi *et al.*, Brain cancer induces systemic immunosuppression through
752 release of non-steroid soluble mediators. *Brain* **143**, 3629-3652 (2020).
753 30. B. T. Himes *et al.*, Use of heparin to rescue immunosuppressive monocyte
754 reprogramming by glioblastoma-derived extracellular vesicles. *J Neurosurg*, 1-11
755 (2022).
756 31. H. Harjunpaa, C. Guillerey, TIGIT as an emerging immune checkpoint. *Clin Exp*
757 *Immunol* **200**, 108-119 (2020).
758 32. N. C. Blessin *et al.*, Patterns of TIGIT Expression in Lymphatic Tissue, Inflammation,
759 and Cancer. *Dis Markers* **2019**, 5160565 (2019).
760 33. J. Yue *et al.*, Myeloid-derived suppressor cells inhibit natural killer cells in
761 myelodysplastic syndromes through the TIGIT/CD155 pathway. *Hematology* **28**,
762 2166333 (2023).
763 34. X. Guan *et al.*, Anti-TIGIT antibody improves PD-L1 blockade through myeloid and
764 T(reg) cells. *Nature* **627**, 646-655 (2024).
765 35. J. H. Han *et al.*, Effective Anti-tumor Response by TIGIT Blockade Associated With
766 FcgammaR Engagement and Myeloid Cell Activation. *Front Immunol* **11**, 573405
767 (2020).
768 36. B. C. Cho *et al.*, Tiragolumab plus atezolizumab versus placebo plus atezolizumab
769 as a first-line treatment for PD-L1-selected non-small-cell lung cancer
770 (CITYSCAPE): primary and follow-up analyses of a randomised, double-blind, phase
771 2 study. *Lancet Oncol* **23**, 781-792 (2022).
772 37. E. Schonfeld, J. Choi, A. Tran, L. H. Kim, M. Lim, The landscape of immune
773 checkpoint inhibitor clinical trials in glioblastoma: A systematic review. *Neurooncol*
774 *Adv* **6**, vdae174 (2024).
775 38. A. Grebe, F. Hoss, E. Latz, NLRP3 Inflammasome and the IL-1 Pathway in
776 Atherosclerosis. *Circ Res* **122**, 1722-1740 (2018).

39. B. Z. Shao, Z. Q. Xu, B. Z. Han, D. F. Su, C. Liu, NLRP3 inflammasome and its inhibitors: a review. *Front Pharmacol* **6**, 262 (2015).
40. K. V. Swanson, M. Deng, J. P. Ting, The NLRP3 inflammasome: molecular activation and regulation to therapeutics. *Nat Rev Immunol* **19**, 477-489 (2019).
41. S. Hamarsheh, R. Zeiser, NLRP3 Inflammasome Activation in Cancer: A Double-Edged Sword. *Front Immunol* **11**, 1444 (2020).
42. B. R. Sharma, T. D. Kanneganti, NLRP3 inflammasome in cancer and metabolic diseases. *Nat Immunol* **22**, 550-559 (2021).
43. R. Kumar *et al.*, Modulating glioma-mediated myeloid-derived suppressor cell development with sulforaphane. *PLoS One* **12**, e0179012 (2017).